TRANSIENT FSI IN A PIPE SYSTEM WITH ELBOW AND TEE JUNCTION

Della J Leslie-Milbourne, Alan E Vardy
Civil Engineering Division, University of Dundee, Dundee DD1 4HN, United Kingdom

Arris S Tijsseling
Department of Mathematics and Computer Science, Eindhoven University of Technology, P.O. Box 513, 5600 MB Eindhoven, The Netherlands

ABSTRACT

Vibrating elbows and Tee-junctions are primary sources of fluid-structure interaction (FSI) in liquid-filled pipe systems; they couple the dynamic behaviour of the liquid and pipes. This paper focuses on a laboratory system with one elbow and one Tee-junction. The stainless steel pipe system is horizontal, closed at its ends and filled with pressurised water. It is suspended on long steel wires to obviate the problem of unknown support conditions. The system is excited by external in-plane impact.

The principal aim of the research was to produce an accurate set of experimental data and the main purpose of this paper is to present and explain the data in a useful form. The measurements include pressures, strains and structural velocities. Representative experimental results are interpreted in detail by means of comparisons with numerical simulations obtained with proven theoretical packages.

1. INTRODUCTION

The underlying mechanisms of FSI in pipes are well understood and, in principle, the phenomenon can be analysed with good accuracy. This is highly dependent on the correctness of the input data defining the system, including geometric and physical properties of the pipes, valves, pumps, supports, etc. In reality, it is rare to be able to prescribe these with high accuracy in a practical application. In fact, it is even rare to be able to do so in controlled, laboratory experiments.

This paper presents experimental data obtained at the University of Dundee. The Dundee laboratory has an excellent history of producing good quality data, with pipe systems purposely designed to obviate the problem of unknown support conditions. The system presently examined, and described in Section 2, uses components from previous configurations and in doing so is beginning to compile a database of related results that enables validation and development of FSI software. The step-wise expansion and development of the experimental apparatus, whilst maintaining as many original components as possible, makes it much easier to identify errors both in the measured data and in the simulating software. Section 3 outlines the theory, Section 4 presents the results and Section 5 gives the conclusions.

2. EXPERIMENT

The experiments were performed at the University of Dundee, using a variation of a system that began development in 1984. Originally designed as a suspended closed single straight pipe, in later stages an elbow and a Tee-junction (together with further pipe sections) have been added to the available components, thus enabling a variety of configurations to be examined.

Previous configurations that have been examined include: single pipe (Vardy & Fan, 1989), single-elbow system (Tijsseling et al, 1996), Tee-junction system (Vardy et al, 1996). The current configuration combines the elbow and Tee-junction system, as illustrated by Figure 2.1.

The system is constructed using stainless steel pipes with an inner diameter of 52 mm and a wall thickness of 3.9 mm. Four pipe sections are used, one of length 4.5 m and three each of length 1.34 m. The two junctions consist of a rigid 90-degree elbow and a rigid Tee-piece. The pipe is closed at the ends and filled with pressurised tap water.

It is suspended by four long (about 3.3 m) thin, vertical steel wires from the ceiling. Two are along pipe 1, one on pipe 3 and one on pipe 4, so that the whole system can move freely in a practically horizontal plane. Great care (in using spirit level, surveying level and theodolite) is taken to ensure that each part of the system is in the same plane. The measured static deflection of the longest pipe caused by its own weight is less than 0.2 mm relative to the suspension points, which are situated about 0.95 m from the pipe ends. Transients are generated by the axial impact of a solid steel rod onto the closed end of the long pipe. The rod is 5 m long and is suspended in a movable frame by means of short steel wires.

The apparatus is less complicated than the

conventional reservoir-pipe-valve system, since 1) an initial steady-state pressure gradient is absent, 2) valve-closure characteristics are not needed and 3) the influence of pipe supports is negligible. Friction and gravity effects are unimportant due to the time scale (milliseconds) of the experiment. Cavitation is avoided by taking a sufficiently high static pressure of the water, usually 2-7 MPa.

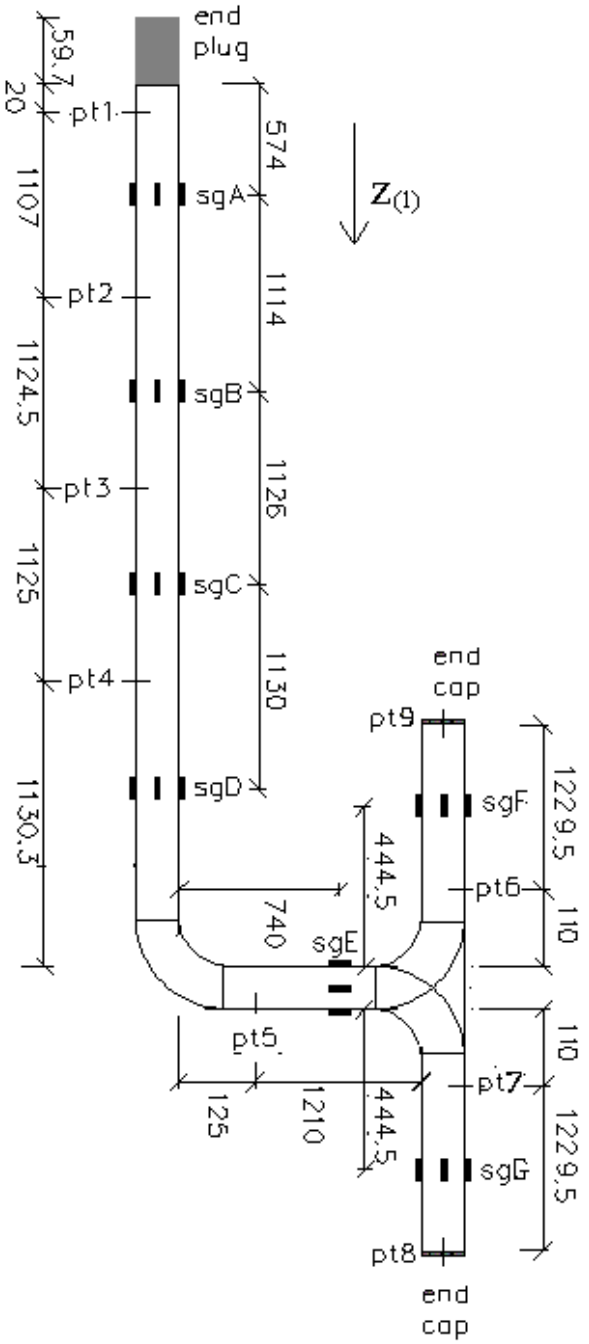

Figure 2.1: Water-filled elbow and Tee-junction pipe system (dimensions in mm) (not to scale).

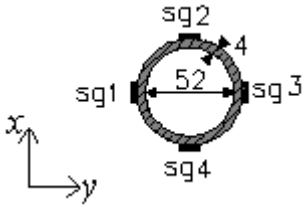

Figure 2.2: Cross-section through pipe illustrating positions of strain gauges.

The pipe is extensively instrumented. Piezoelectric pressure transducers (Kistler 7031, 701A) are mounted (with their diaphragms flush with the inner wall of the pipe) near to the impact end, at the remote ends and at six intermediate points, as indicated in Figure 2.1. The transducers are acceleration-compensated and have an observed rise time of 0.15 ms (Fan 1989, p. 20), or 0.2 ms/MPa, and a natural frequency of 80 kHz. The connected amplifiers (Fylde FE428CA) have a cut-off frequency of 50 kHz. Strain gauges (TML-FRA-1-11) are attached to the pipe wall at four locations along the long pipe and at one location along each of the shorter pipes. At each location, four three-way (axial, hoop, shear) strain gauges are equidistantly placed around the pipe circumference as sketched in Figure 2.2. The connected amplifiers (Fylde FE458AC) have a cut-off frequency of 70 kHz. A laser-Doppler vibrometer (Dantec DISA 55X) is used for non-contact measurements of one-directional pipe wall velocities at one selected location. Furthermore it is used to determine the impact velocity of the rod. The connected amplifier (DISA 55N21, 55N11) has a cut-off frequency of 26 kHz. The measured signals are fed into two data acquisition systems (with in total 22 channels) at sampling rates up to a maximum of 1 MHz per channel.

The physical dimensions and material properties of the pipe, water and rod are given in Table 2.1, together with the measuring positions of the pressure transducers (PT), strain gauges (SG) and laser-Doppler vibrometer (LDV). The method of measurement and the accuracy of the values in Table 2.1 are given in (Fan 1989, p. 28; Fan & Tijsseling 1992, p. 269). The masses m_1, m_2 and m_3 of the end plug and end caps, respectively, which close the pipe, are normally incorporated in the simulations. The dimensions of the end pieces and the mass of the attached instrumentation, given by Fan (1989, p. 29 and p. 16, respectively), are neglected. The influence of the inertia of the end pieces, which can be assessed from the empty-pipe measurements of Fan (1989, pp. 41-42), is neither negligible nor dominant.

In the absence of cavitation, the underlying theory (given in Section 3) is linear. The pressures,

velocities and strains are then linearly proportional to the impact velocity of the rod, so that measurements for one particular impact velocity are considered to be sufficient.

The results presented in Section 4 are only a small sample of those obtained. A total of 49 experiments were performed, providing almost 800 measured signals.

Water-filled pipe	Position of instrumentation along each pipe	Solid steel rod
L_1 = 4.51 m	*Pipe 1:*	L_r = 5.006 m
L_2 = 1.34 m	z(PT1) = 0.0195 m	R_r = 25.37 mm
L_3 = 1.34 m	z(PT2) = 1.1265 m	E_r = 200 GPa
L_4 = 1.34 m	z(PT3) = 2.2510 m	ρ_r = 7848 kg/m^3
R = 26.01 mm	z(PT4) = 3.3760 m	V_{0r} = 0.3 m/s
e = 3.945 mm	z(SGA) = 0.5740 m	Except for Figure 4.5:
γ = 0	z(SGB) = 1.6880 m	V_{0r} = 0.8 m/s
K = 2.14 GPa	z(SGC) = 2.8140 m	
ρ_f = 999 kg/m^3	z(SGD) = 3.9440 m	
E = 168 Gpa	z(LDV) = 0.0465 m	
G = 65.1 GPa	*Pipe 2:*	
κ^2 = 0.53	z(PT5) = 0.125 m	
ρ_t = 7985 kg/m^3	z(SGE) = 0.74 m	
ν = 0.29	*Pipe 3:*	
m_1 = 1.30 kg	z(PT6) = 0.11 m	
m_2 = 0.32 kg	z(PT9) = 1.34 m	
m_3 = 0.32 kg	z(SGF) = 0.445 m	
m_{elbow} = 0.88 kg	*Pipe 4:*	
m_{Tee}	z(PT7) = 0.11 m	
	z(PT8) = 1.34 m	
	z(SGG) = 0.445 m	

Table 2.1: Elbow and Tee-junction pipe experiment; input data for simulations.

3. THEORY

The equations used to model FSI are well developed. An 8-equation model, as described by Wiggert et al (1987) and Wiggert & Tijsseling (2001), is used for the planar system under consideration. It includes a 4-equation model for the fluid velocity V, fluid pressure P, axial pipe velocity $\dot{u}_z$ and axial pipe stress σ_z, governing axial motion:

$$\frac{\partial V}{\partial t}+\frac{1}{\rho_t}\frac{\partial P}{\partial z}=0. \tag{1}$$

$$\frac{\partial V}{\partial z}+\frac{1}{\rho_t {c_F}^2}\frac{\partial P}{\partial t}=2\nu\frac{\partial \dot{u}_z}{\partial z} \tag{2}$$

$$\frac{\partial \dot{u}_z}{\partial t}-\frac{1}{\rho_t}\frac{\partial \sigma_z}{\partial z}=0. \tag{3}$$

$$\frac{\partial \dot{u}_z}{\partial z}-\frac{1}{\rho_t {c_t}^2}\frac{\partial \sigma_z}{\partial t}=-\frac{\rho_f}{\rho_t}\frac{\nu R}{Ee}\frac{\partial P}{\partial t} \tag{4}$$

in which

$${c_F}^2=\left(\rho_f\left(\frac{1}{K}+\left(1-\nu^2\right)\frac{2R}{Ee}\right)\right) \tag{5}$$

and

$${c_t}^2=\frac{E}{\rho_t} \tag{6}$$

are the squares of the fluid and solid wave speeds, respectively; and a 4-equation model for lateral pipe velocity $\dot{u}_y$, shear force Q_y, rotational pipe velocity $\dot{\theta}_x$ and bending moment M_x, governing lateral motion:

$$\frac{\partial \dot{u}_y}{\partial t}+\frac{{c_s}^2}{\kappa^2 GA_t}\frac{\partial Q_y}{\partial z}=0. \tag{7}$$

$$\frac{\partial \dot{u}_y}{\partial z}+\frac{1}{\kappa^2 GA_t}\frac{\partial Q_y}{\partial t}=-\dot{\theta}_x \tag{8}$$

$$\frac{\partial \dot{\theta}_x}{\partial t}+\frac{{c_b}^2}{EI_t}\frac{\partial M_x}{\partial z}=\frac{1}{\rho_t I_t}Q_y \tag{9}$$

$$\frac{\partial \dot{\theta}_x}{\partial z}+\frac{1}{EI_t}\frac{\partial M_x}{\partial t}=0 \tag{10}$$

in which

$${c_s}^2=\frac{\kappa^2 GA_t}{\rho_t A_t+\rho_f A_f} \tag{11}$$

and

$${c_b}^2=\frac{E}{\rho_t} \tag{12}$$

are the squares of the shear and bending wave-front speeds, respectively.

Boundary conditions for unrestrained closed ends are given by:

$$V = \dot{u}_z, \tag{13}$$

$$A_t \sigma_z \pm m\ddot{u}_z = A_f P, \tag{14}$$

$$Q_y = M_x = 0. \tag{15}$$

For the impact end, during the period of contact between pipe and rod, condition (14) is replaced by

$$A_t \sigma_z \pm m\ddot{u}_z = A_f P + A_r \sqrt{E_r \rho_r}\,(V - V_{0r}) \tag{16}$$

where V_{0r} is the velocity of the rod just before impact. At the elbow and the Tee-junction, local conditions prescribing continuity and equilibrium couple the axial equations (1)-(4) to the lateral equations (7)-(10).

4. RESULTS

Experimental results obtained for the system described in Section 2 are compared with numerical simulations based on the theory in Section 3. The numerical results presented in this subsection were obtained with the ALT-code (in-house software developed by the first author) which automatically calculated the required computational grids (two for each pipe) using small adjustments in the mass densities to avoid the need for interpolation.

The reproducibility of the experiments is examined in Figure 4.1, showing dynamic pressures measured at the impact end in two successive runs. This shows excellent reproducibility, with it being practically impossible to distinguish between the two sets.

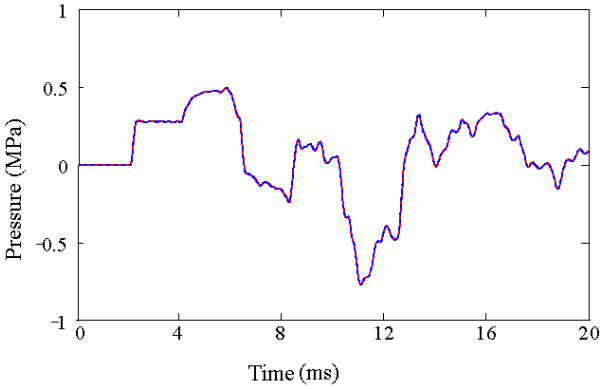

Figure 4.1: Reproducibility of elbow and Tee-piece system; pressure near impact end (PT1).

Figures 4.2-4.7 compare experimental with numerical data. In each figure, experimental data are given by the solid/red line and numerical data by the dashed/blue line. The first 20 ms after impact are shown.

Figures 4.2-4.4 show measured and calculated pressures near to the impact end (PT1), near to the elbow (PT5) and at one of the remote ends (PT9). In each figure, there is a good correlation (sufficient consistency) between experimental and numerical work. The arrivals of the main wave fronts can be recognised in the pressure traces. However, because the elbow and Tee-junctions give rise to lateral waves, the interpretation is difficult due to the dispersive character, and hence non-constant propagation speeds, of lateral wave trains. The impact of the rod creates a pressure wave in the liquid and a stress wave in the pipe wall. This initial jump can be seen as the first pressure rise in Figure 4.2. The second pressure rise takes place at approximately 2 ms after the initial impact, the time required for the stress wave to travel along the long pipe to the elbow and be reflected back. The rounding of this pressure rise is because the axial motion of the long pipe is retarded at the elbow by lateral inertia forces in the second pipe. The results for a single straight pipe would show a much squarer response. The stress wave travels 3.4 times faster than the pressure wave, so that at the elbow the pressure is seen to fall (see Figure 4.3) due to the arrival of the stress wave pushing the elbow in the positive $z_{(1)}$-direction. The axial stress wave in the solid causes a pressure change in the liquid (because of Poisson contraction). Because this travels in front of the main pressure wave, it is often referred to as a precursor wave. The arrival of the main pressure wave, some 2.4 ms later, signifies the pressure increase. Between these two events, fluctuations are due to reflected waves from the Tee-junction and lateral wave effects. Similarly, at the remote end (Figure 4.4), the first response seen is the arrival of a stress (precursor) wave at about 1.3 ms after the initial impact, before the large pressure drop generated at the elbow arrives. This event, however, is less distinct due to the complex wave behaviour. During the following 4-5 ms, several pressure changes can be observed before the original pressure wave arrives causing the positive dynamic pressure.

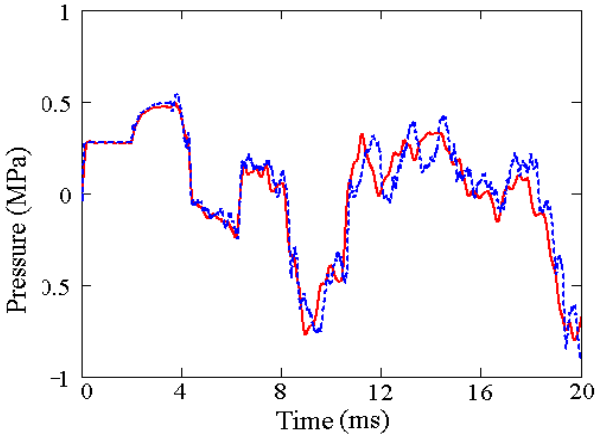

Figure 4.2: Measured (——) and calculated (- - -) dynamic pressure near impact end (PT1).

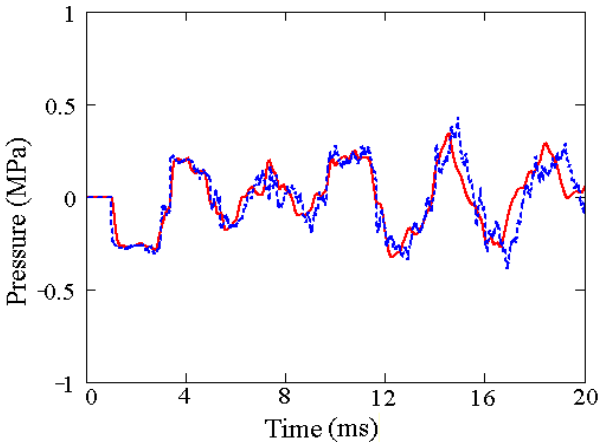

Figure 4.3: Measured (——) and calculated (- - -) dynamic pressure near elbow (PT5).

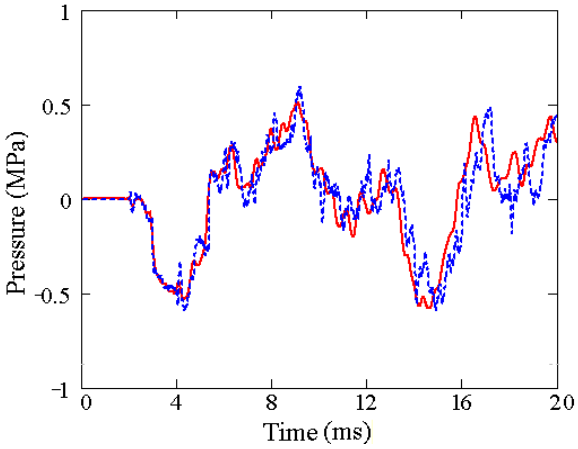

Figure 4.4: Measured (——) and calculated (- - -) dynamic pressure at remote end (PT9).

Axial pipe wall velocities, measured and calculated near the impact end are shown in Figure 4.5. Because these are so close to the closed end, where $V = \dot{u}_z$, they are also representative of the fluid velocity. The first few milliseconds closely resemble the traces given by the pressure measurements. This is due to the strong coupling between the fluid and solid at the pipe end and because of the Joukowsky relation: $\Delta P = \rho_f \, c_F \, \Delta V$.

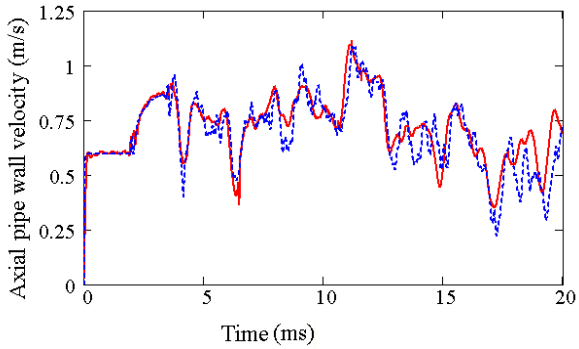

Figure 4.5: Measured (——) and calculated (- - -) axial pipe wall velocity near impact end.

Axial strains, measured and calculated at position A (0.57 m from the impact end) on the long pipe (see Fig. 2.1), are shown in figure 4.6. The large compression of about 2 ms duration at the beginning defines the period of energy transfer from the impact rod to the pipe system, the rod and pipe being in contact during these 2 ms. Rod-pipe separation occurs after the travelling axial stress wave in the long pipe has returned from the elbow.

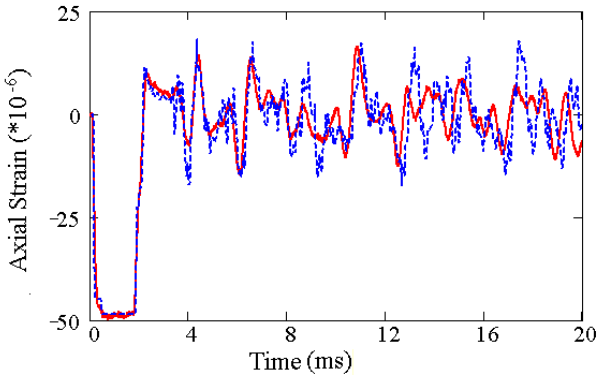

Figure 4.6: Measured (——) and calculated (- - -) dynamic axial strain at position A.

Figure 4.7 shows measured and calculated bending moments at position A. Measured bending moments are determined from the difference between axial strains measured on opposite faces of the pipe according to the formula:

$$M_x = \frac{E I_t}{2(R+e)} \left\{ \varepsilon_z^{(1)} - \varepsilon_z^{(3)} \right\} \qquad (17)$$

where I_t is the second moment of area of the pipe cross-section about the x-axis (see Fig. 2.2). The figure nicely exhibits frequency dispersion; small,

high frequency oscillations can be seen before the arrival of larger oscillations. Detailed discussion of events in these results is difficult due to the dispersive characteristic of lateral wave trains, as mentioned previously. Overall agreement between observed values and the predictions is reasonable.

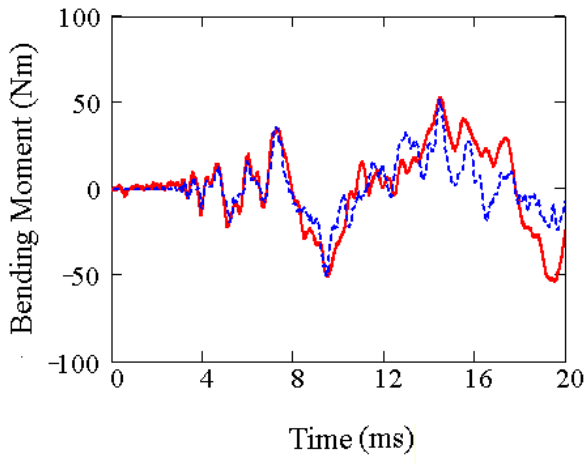

Figure 4.7: Measured (——) and calculated (- - -) dynamic Bending Moment at position A.

5. CONCLUSIONS

1. An experimental facility with a history of providing simple measurements of FSI phenomena in suspended pipes has been extended to include a combination of an elbow and a Tee-junction.
2. Extensive measurements have been made in the apparatus, giving data describing pressures, strains and velocities at regularly-spaced locations along the pipes.
3. Sufficient measurements have been presented herein to enable a clear picture of the nature of the measurements to be conveyed. The repeatability of the measurements has been demonstrated and key features have been highlighted by comparison with theoretical predictions.
4. The basis of a theoretical method has been summarised and sufficient comparisons have been made to demonstrate its ability to reproduce the main features of the experimental measurements. There is insufficient space herein for a detailed, critical validation of the theoretical model, but the comparisons provide strong supporting evidence that the data are meaningful.
5. In total, 49 experiments have been undertaken to provide new data for researchers seeking to understand FSI and/or to validate predictive software. The published data will be made available through the Surge-Net FSI web site www.win.tue.nl/fsi.

6. ACKNOWLEDGEMENTS

The Surge-Net project (http://www.surge-net.info) is supported by funding under the European Commission's Fifth Framework 'Growth' Programme via Thematic Network "Surge-Net" contract reference: G1RT-CT-2002-05069. The authors of this paper are solely responsible for the content and it does not represent the opinion of the Commission. The Commission is not responsible for any use that might be made of data herein.

Colin Stark and Ernie Kuperus are thanked for technical assistance in running the experimental apparatus.

7. REFERENCES

Fan D, 1989. Fluid-structure interactions in internal flows. Ph.D. Thesis, The University of Dundee, Department of Civil Engineering, Dundee, UK.

Fan, D., Tijsseling, A., 1992. Fluid-structure interaction with cavitation in transient pipe flows. *ASME Journal of Fluids Engineering* **114**, 268-274.

Tijsseling AS, Vardy AE, and Fan D, 1996. Fluid-structure interaction and cavitation in a single-elbow pipe system. *Journal of Fluids and Structures* **10**, 395-420.

Vardy AE and Fan D, 1989. Flexural waves in a closed tube. In *Proceedings of the 6th International Conference on Pressure Surges, BHRA,* Cambridge, UK, 43-57.

Vardy AE, Fan D, and Tijsseling AS, 1996. Fluid/structure interaction in a T-piece pipe. *Journal of Fluids and Structures* **10**, 763-786.

Wiggert DC, Hatfield FJ, Stuckenbruck S, 1987. Analysis of liquid and structural transients by the method of characteristics. *ASME Journal of Fluids Engineering* **109**, 161-165.

Wiggert DC, Tijsseling AS, 2001. Fluid transients and fluid-structure interaction in flexible liquid-filled piping. *ASME Applied Mechanics Reviews* **54**, 455-481.